Pramana – J. Phys. (2018) 90:37
https://doi.org/10.1007/s12043-017-1519-4

First principles calculations of optical properties of the armchair SiC nanoribbons with O, F and H termination

DAO-BANG LU[1,2] and YU-LING SONG[3,*]

[1]College of Mechanical and Electronic Engineering, Nanyang Normal University, Nanyang 473061, China
[2]Henan Engineering Laboratory of Petroleum Equipment Intelligent Control, Nanyang 473061, China
[3]College of Physics and Electronic Engineering, Nanyang Normal University, Nanyang 473061, China
[*]Corresponding author. E-mail: yuling985@163.com

MS received 11 April 2017; revised 30 August 2017; accepted 3 October 2017; published online 13 February 2018

Abstract. Based on density functional theory, we perform first-principles investigations to study the optical properties of the O-, F- and H-terminated SiC nanoribbons with armchair edges (ASiCNRs). By irradiating with an external electromagnetic field, we calculate the dielectric function, reflection spectra, energy loss coefficient and the real part of the conductance. It is demonstrated that the optical constants are sensitive to the low-energy range, different terminal atoms do not make much difference in the shape of the curves of the optical constants for the same-width ASiCNR, and the optical constants of wider nanoribbons usually have higher peaks than that of the narrower ones in low energy range. We hope that our study helps in experimental technology of fabricating high-quality SiC-based nanoscale photoelectric device.

Keywords. First-principles; optical properties; termination; SiC nanoribbon.

PACS Nos 61.48.+c; 73.61.Wp; 78.66.−w

1. Introduction

Because of their unique properties, low-dimensional nanomaterials have become a hot topic in recent research, such as zero-dimension (0D) nanoclusters [1], one-dimensional nanolines [2] and two-dimensional (2D) graphite-like materials [3–5]. Based on density functional theory (DFT) calculations, Chowdhury *et al* studied the pseudo-Jahn–Teller distortion in phosphorene (Pn) and they found that Pn showed a much richer phase diagram [4]. Ever since the synthesis of high-quality graphene, a single layer carbon sheet with a honeycomb structure, quasi-one-dimensional nanomaterials which are called nanoribbons, are always the focus due to their excellent physical and chemical performances [6–10].

Among the large number of semiconductor materials, SiC nanomaterials, because of the advantages of the wide energy gap, high breakdown critical field and thermal conductivity, small dielectric constant, high electron mobility, excellent mechanical properties, etc., are expected to be ideal materials for designing electronic and optoelectronic devices with high frequency, high power, low energy consumption, high temperature resistance and radiation resistance [11–17]. SiC nanomaterials have novel and immense application prospects for the microelectronic devices and the large-scale integrated circuit. Therefore, studying SiC nanomaterials has recently attracted much attention of the researchers.

Because of the excellent physical properties and their potential applications in optoelectronics, researchers have been trying to prepare ideal SiC nanomaterials. In the past decade, a large variety of SiC nanostructures have been successfully synthesised, including nanocrystals [18], nanowires [19], nanoribbons [11], and so on. In 2012, He *et al* prepared large-scale SiC nanocrystals with several nanometers using direct chemical etching method [18]. By using the vapour–liquid–solid (VLS) mechanism starting with the catalytic Fe droplets at 1500°C, Feng *et al* precisely controlled the growth of β-SiC nanowires [19]. Using different methods, researchers synthesised SiC nanoribbons with tens of nanometer thickness [11,20,21].

On the other hand, theoretical studies also get great progresses. In the past few years, extensive researches on SiC nanomaterials have focussed more on the quasi-one-dimensional honeycomb structure, that is SiC nanoribbons (SiCNRs) [22–27]. Up to now, the study of the

electronic and magnetic properties is still the most popular topic. Various factors can influence the electronic and magnetic properties, including the width and the edge shape of the nanoribbons, intrinsic defects, the edge termination atoms, the electric field, etc. For example, by using first-principles computations, Guan *et al* [22] demonstrated that electronic and magnetic properties of SiCNRs can be greatly achieved by controlling the hydrogenation pattern and ratio; Ding and Wang [25] studied the electronic and magnetic properties of the zig-zag SiC nanoribbons (ZSiCNRs) with asymmetric H terminations and terminal SiC/C edge, respectively. They found that the asymmetric H atoms or the terminal Si/C edge has enormous impact on the electronic and magnetic properties of ZSiCNRs; Du *et al* found that the band gaps of ZSiCNRs decrease monotonically with the transverse strength of field E [28].

In the study of these fields, most researchers choose H atom as the terminal atom of the dangling bonds at the edges of the SiCNRs (SiCNRs-H). By using sophisticated methods like GW approximation and Bethe–Salpeter equation (BSE), Alaal *et al* studied the structure and optical properties of SiC nanoribbons with and without hydrogen termination, and they found that the absorption spectra are modified significantly [29]. However, some theoretical studies show that the terminal F and O atoms can affect the electronic and magnetic properties of the nanomaterials [30–32]. Recent theoretical research has also focussed on fluorinated nanomaterials [33,34]. In this work, using the first-principles projector-augmented wave (PAW) potential within the DFT framework under the generalised gradient approximation (GGA), we report for the first time a systematic theoretical investigation of the electronic and optical properties of SiCNRs-F, -H and -O with armchair edge (ASiCNRs).

2. Calculation method and structure model

Our calculations are carried out in the framework of the DFT [35–38], as performed in the plane-wave-basis-set Vienna *ab initio* package (VASP). The electron–ionic core interaction is represented by the PAW potentials [39]. We chose GGA with the Perdew–Burke–Ernzerhof (PBE) formulation [40] to describe the electron exchange and correlation, which developed the calculations of the combined systems. The cut-off energy is set to 450 eV for the plane waves, and further increasing the value has little effect on the results. The sampled k points $20\times1\times1$ are used to sample the one-dimensional Brillouin zone in order to obtain the electronic properties. To avoid the numerical instability due to level crossing and quasidegeneracy near the Fermi level, we use Gaussian smearing method and a width of 0.05 eV. Geometric structures of SiCNRs are fully relaxed to minimise the total energy and forces acting on each atom smaller than 10^{-5} eV and 0.01 eV/Å.

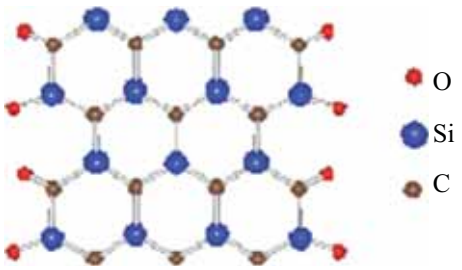

7-ASiCNR

Figure 1. Geometric structure of 7-ASiCNR-O. The red, blue and brown balls represent O, Si and C atoms, respectively.

Figure 1 presents the quasi-one-dimensional atomic structure of ASiCNR-O. Using the same definition as before, the width of ASiCNR is classified by the number of the dimer lines (N_a) across the ribbon width, defined by N_a-ASiCNR (as shown in figure 1, $N_a = 7$). We use super-cell geometry to simulate infinite long isolated nanoribbon. To avoid the interaction of the neighbouring ribbons, the ASiCNRs are separated from each other by a distance of at least 20 Å in both edge-to-edge and layer-to-layer directions.

3. Results and discussions

Before this, we have completed the calculation of the structure and the electronic properties of SiC nanoribbons with F and H termination [41]. For comparing and analysing the influence of the terminal O atoms to the structure, electronic and optical properties of 7-ASiCNR, we also give some previous results. The optimised average bond lengths of Si–C, Si–H, C–H, Si–F, C–F, Si–O and C–O are 1.79, 1.49, 1.09, 1.59, 1.38, 1.54 and 1.22 Å, respectively. The bond lengths of Si–C, Si–H and C–H are calculated in accordance with those in ref. [29].

Figures 2a–2c present the band structures of 7-ASiCNRs-F, -H and -O. Figures 2d and 2e show the total density of state (DOS) of 7-ASiCNR-O and the charge densities as well as the cross-section from top to bottom for the four selected bands nearest to the Fermi level shown in orange, blue, violet and green bands of 7-ASiCNR-O. The local DOS (LDOS) onto the O, C and Si atoms of 7-ASiCNR-O are plotted in figure 3. One can see that in figures 2a–2c, similar to the results of 7-ASiCNRs-F and -H, the edge state do not

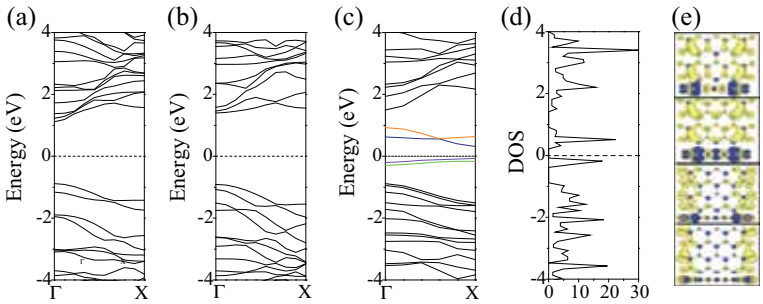

Figure 2. Band structures of (**a**) 7-ASiCNR-F, (**b**) 7-ASiCNR-H and (**c**) 7-ASiCNR-O, (**d**) the total DOS of 7-ASiCNR-O and (**e**) the charge densities as well as the cross-section from top to bottom for the four selected bands nearest to the Fermi level shown in orange, blue, violet and green bands of 7-ASiCNR-O. In the cross-section plots of the charge densities, the colour from blue to red represents the value of charge density in increasing order. The Fermi level is set to zero and indicated by the black dashed lines.

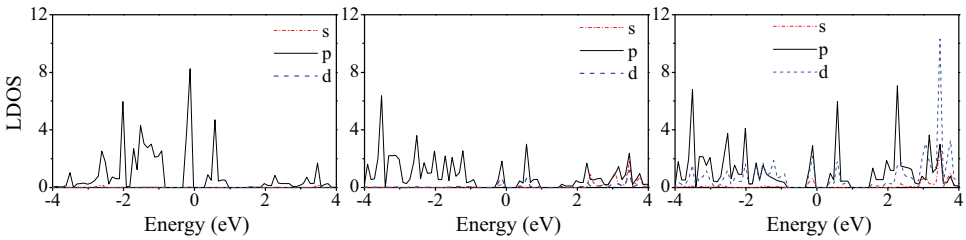

Figure 3. LDOS onto the (left) O atom, (centre) C atom and (right) Si atom of 7-ASiCNR-O.

present in 7-ASiCNR-O due to its specific dimer edges. So, just looking at the band structure of 7-ASiCNR-O, we can see that 7-ASiCNR-O represents a direct semiconducting character too, but its band gap (0.39 eV) is smaller than that of 7-ASiCNRs-F (2.0 eV) and -H (2.31 eV), and the band gap results in a valley at the Fermi level in the total DOS in figure 2d. Compared to the band structures of the ASiCNR-F and ASiCNR-H, the nearest four colour bands to the Fermi level are impurity-induced bands, which are mainly contributed to by the hybridised states of the terminated O atom and the neighbouring Si and C atoms. At the same time, we have given corresponding charge densities of the aforementioned four colour bands, as shown in figure 2e. One can see, from the charge densities, that the two conduction bands are mainly from the π electrons of the O, Si and C atoms, while the two valence bands are mainly from the σ electrons of the O and the edge Si and C atoms. Compare the total DOS with the LDOS shown in figure 3, one can also see that p orbitals of the O atoms contribute most to the four bands nearest to the Fermi level, especially to the valence bands. The main contribution of p orbital for C atoms lies in the lower level of the valence band, while the small contribution of s and d orbitals for C atoms lies in the higher level of the conduction band. However, the p orbital of Si atoms contributes greatly to the valence and conduction bands, the d orbital of Si atoms contributes more to the conduction than to the valence bands, the s orbital contributes less to the conduction band. Moreover, in figure 3 for each first peak at the side of the valence and conduction band, the p orbital of O, C and Si atoms shows a strong hybridisation, and the C-p and Si-p at -3.5, -2.6, -2.0, 2.4, 3.2 and 3.6 eV, Si-p, d orbitals at 3.6 eV show a strong hybridisation, too. In summary, band structures and the total DOS of 7-ASiCNR near the Fermi level are mainly decided by the p electrons of the atoms and the d electrons of the Si atoms, and thus the electrical transport properties and the types of the carriers near the Fermi level are mainly decided by the p electrons of the atoms and the d electrons of the Si atoms. It is the same for 13-ASiCNR also.

And just as the band gaps vary with the width of the ASiCNRs-F and -H [41], the band gaps of ASiCNR-O also vary with different bandwidths. The band structures of 13-ASiCNRs-F, -H and -O as well as the total DOS of 13-ASiCNR-O are plotted in figure 4. We can see that the band gaps of 13-ASiCNRs-F and -H are 2.10 and 2.32 eV, and the band gap of 13-ASiCNR-O increases to 0.56 eV because the lowest conduction band moves up, and thus in the LDOS the first peak in the side of the conduction band also moves. Comparing the LDOS in figure 5 with the one in figure 3, one can see that the LDOS onto the O, C and Si atoms

of 13-ASiCNR-O are remarkably similar to those of 7-ASiCNR-O, except for the amplitude. Moreover, as the bandwidth increases, the number of Si–C bonds will certainly also increase, and thus the density of the energy band increases, too, which can be seen from the band structures and total DOS in figure 4. Similar to the hybridisation in figure 3, each of the first peak at the side of the valence and conduction bands of the O-p, C-p and Si-p orbitals show less hybridisation, and the C-p and Si-p at -3.3 eV, Si-p, d orbitals at -3.3 and 3.2 eV show strong hybridisation. Moreover, from the band structures and the total DOS or LDOS shown in figures 2, 3, 4 and 5, the Fermi level of ASiCNR-O moves to the top of the valance band. The ASiCNR-O system shows p-type semiconductor properties.

Figure 6 shows the band gap as a function of the ribbon width N_a for ASiCNRs-H and -O. From figure 6, we can see that for the same ribbon width, ASiCNR-H has band gaps bigger than those of ASiCNR-O. The band gaps quench to the constant values of 2.36 and 0.59 eV for ASiCNRs-H and -O, respectively. The band gaps for ASiCNR-H exhibit the family behaviour following the heirachy $3p>3p+1>3p+2$, which is in good agreement with the DFT band gaps in ref. [29]. For examples, in ref. [29], when $N_a = 6$, 7 and 8, the band gaps are 2.41, 2.38 and 2.31 eV, respectively and our results are 2.37, 2.34 and 2.27 eV, respectively. The band gaps of ASiCNR-O display different oscillating behaviours, and the band gaps follow the hierarchy $2p>2p+1$ which are quite unlike AAlNNR-O presenting a semimetallic property [42].

The chief bands which become the dominant factor in defining optical properties are in the infrared and visible light range because almost all the band gap energies of the semiconductor are within this wavelength ranges, and so do the band gap energies of ASiCNRs. The wavelength of the infrared and visible light range is considerably larger than lattice constants of nanosemiconductor, and so the solid materials' optical properties usually are characterised by macro-optical constants, such as reflectivity, energy loss coefficient, conductance, etc. Of all the optical constants, refractive index (n) and extinction coefficient (k) are perhaps the most fundamental, which are functions of the photon energy of frequency. The relation between constants n and k with the complex dielectric function $\varepsilon(\omega) = \varepsilon_1(\omega) + i\varepsilon_2(\omega)$ is presented as follows:

$$\varepsilon_1(\omega) = n^2 - k^2 \quad (1)$$

$$\varepsilon_2(\omega) = 2nk. \quad (2)$$

The microcosmic physical process between interband transition and solid electronic structure can be expressed in dielectric function, from which we can also get various other spectra information. The imaginary and real parts of the 7- and 13-ASiCNRs-F, -H and -O are presented in figures 7 and 8, respectively.

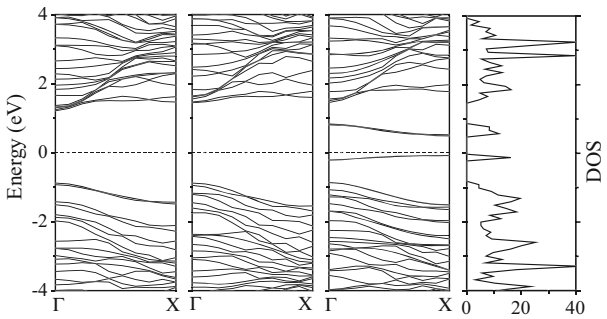

Figure 4. From the left to the right panels, band structures of 13-ASiCNRs-F, -H and -O as well as the total DOS of 13-ASiCNR-O are shown. The Fermi level set to zero is indicated by black dashed lines.

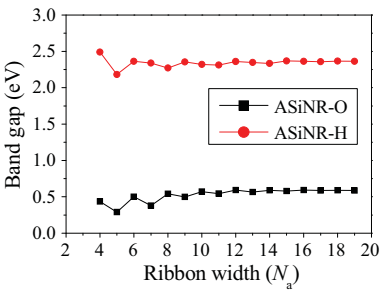

Figure 6. Variation of the energy band gap as a function of the ribbon width N_a for ASiCNRs-O and -H.

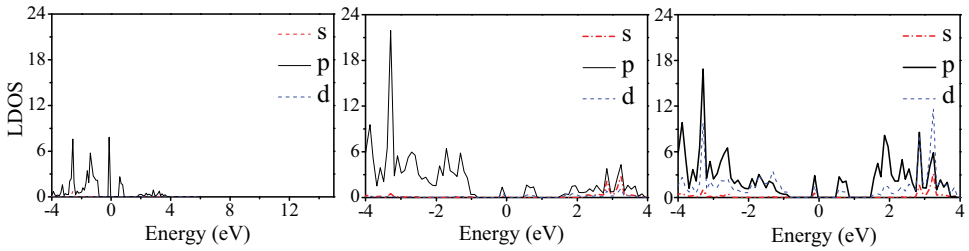

Figure 5. LDOS onto the (left) O atom, (centre) C atom and (right) Si atom of 13-ASiCNR-O.

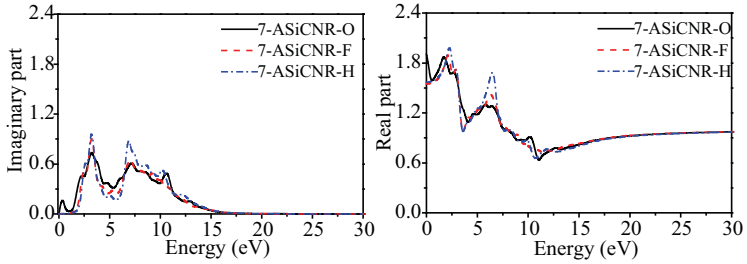

Figure 7. The theoretically calculated dielectric functions of 7-ASiCNRs-F, -H and -O.

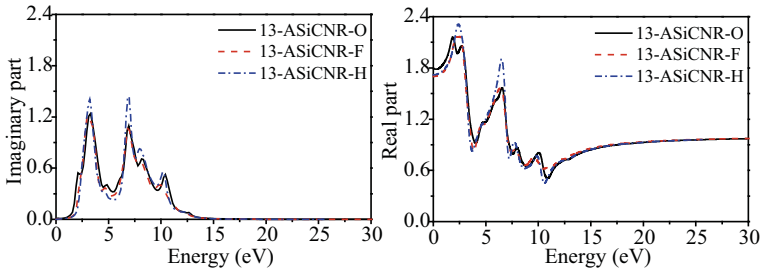

Figure 8. The theoretically calculated dielectric functions of 13-ASiCNRs-F, -H and -O.

First, the curves of the imaginary and real parts have exactly similar shape no matter what atoms are terminated when the nanoribbons have the same bandwidth and amplitude. By contrast, the wider nanoribbon usually has a higher peak than the narrower one in the infrared and visible light range because the former has more electrons than the latter. From the above, we can understand that they have the same transition mechanism, and thus we shall not discuss each of these nanoribbons in detail, we shall discuss about only one width, and other optical constants for one kind of edge shape.

Secondly, the spectra of ASiCNRs are produced by electronic transitions between their bands, and thus the dielectric constant peaks can be explained by their density of states and band structures. All the dielectric constant peaks are located at the low-energy range, whether to the imaginary and the real parts or to the different bandwidths and different terminal atoms. The first dielectric peak of 7-ASiCNR-O locates at 0.39 eV corresponding to the interband transitions from the highest valence band to the lowest conduction band at the X point. The following two maximum peaks correspond to the photon energies of 3.31 and 7.20 eV, respectively; the former is produced by the transitions from the fourth valence band to the sixth conduction band, while the latter from tenth valence band to the thirteenth conduction band (valence and conduction bands are counted from the Fermi level). These photon energies are all one-to-one match to the corresponding peak values in the DOS. By comparing the imaginary and real parts of 7-ASiCNR-H and 7-ASiCNR-F with 7-ASiCNR-O, we can see that the position of the two maximum peaks are roughly corresponding to each other, only the peaks have a slightly blue shift and the values are stronger.

Thirdly, from the left panels of figures 7 and 8, we can see that the value of the imaginary parts of 7- and 13-ASiCNRs is zero at higher incident energy (higher than 17 eV for 7-ASiCNR, 14 eV for 13-ASiCNR). The imaginary part describes the transition between the occupied valance bands and the unoccupied conduction bands. That is, at higher incident energy area, electron transition does not occur, and thus the systems are optically transparent. At the high energy range, the real parts incline to a constant irrespective of the terminal atoms. Moreover, from the real parts in the right panel of figure 7, we can see that the zero frequency dielectric constant of 7-ASiCNRs-O (1.91) is slightly larger than those of -F (1.57) and -H (1.55), indicating that 7-ASiCNR-O can be a dense refraction material applied in optoelectronics.

The reflection spectra, energy loss coefficients and real parts of the conductance of 7- and 13-ASiCNRs-F, -H and -O are presented in figures 9, 10 and 11, respectively. From these figures, we can see that the spectra are mainly in the low-energy areas which are extremely similar to the changing trends of the imaginary parts of the dielectric functions, while in the high energy range, the spectra are almost zero.

The reflection spectrum is the most direct manifestation of the energy band and all the reflection peaks belong to different interband transitions. Figures 7 and 8 are the imaginary and real parts of 7- and

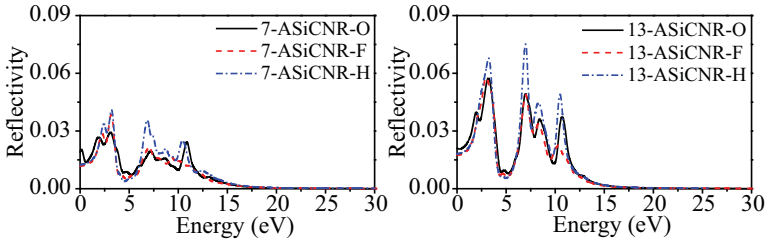

Figure 9. The theoretically calculated reflection spectra of 7- and 13-ASiCNRs terminated with O, F and H atoms.

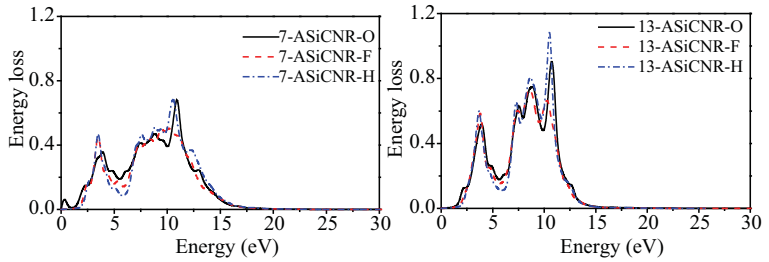

Figure 10. The energy loss coefficient of O-, F- and H-terminated 7-ASiCNRs and 13-ASiCNRs. The black solid, red dashed and blue dashed dot lines indicate the energy-loss coefficients of O-, F- and H-terminated ASiCNRs, respectively.

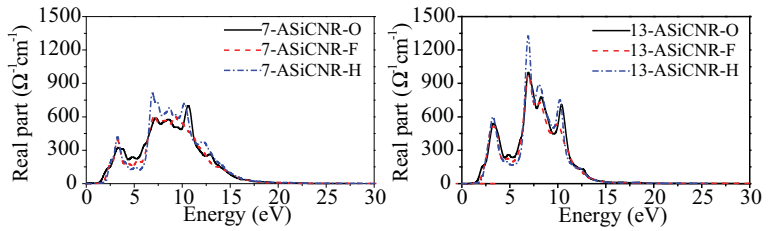

Figure 11. Real part of the conductance of O-, F- and H-terminated 7-ASiCNRs and 13-ASiCNRs. The black solid, red dashed and blue dashed dot lines indicate the conductance of O-, F- and H-terminated ASiCNRs, respectively.

13-ASiCNRs-F, -H and -O, respectively. Comparing figure 9 with figures 7 and 8, we can see that the reflection peaks correspond to the dielectric peaks, which is the macroscopic expression of the interband transition behaviour, that is, the transition mechanism of the reflection peaks is consistent with that of the dielectric spectrum, and so do the energy loss coefficients and real parts of the conductance. In figure 9, even for the strongest reflectivity, the value is smaller than 8% irrespective of whether the bands are narrower or wider. Moreover, in the energy range 1.6–3.0 eV (visible range) the reflectivity is even lower. So, we can say that the systems can be seen as optically transparent in the visible range.

The energy loss function is also an important factor describing the energy loss of the electrons traversing in a material. This can be obtained from the dielectric function by the expression $L(\omega) = \varepsilon_2(\omega)/(\varepsilon_1^2(\omega) + \varepsilon_2^2(\omega))$. The peaks of the energy loss represent the properties related to the plasma resonance and the oscillation frequency is called plasma frequency which is consistent with the trailing edges in the reflection spectra [43]. That is, the narrower are the trailing edges, the higher are the energy loss peaks. In figure 10, for instance, the last energy loss peaks of 7-ASiCNR-O and 13-ASiCNR-O are at about 10.76 and 10.90 eV which correspond to the last abrupt reductions at 10.71 and 10.76 eV in the reflection spectra of 7-ASiCNR-O and 13-ASiCNR-O in figure 9 respectively.

The real part of the conductance of O-, F- and H-terminated 7-ASiCNRs-O and 13-ASiCNRs-O vs. photon energy are presented in figure 10. In an external irradiation field, a transition from the valence band to the conduction band will occur when a direct absorption photon with irradiation energy is present in the horizontal axis, and where a peak will appear in the real part of the conductance in the corresponding position [44]. For instance, several obvious absorption peaks at 3.30, 4.86, 6.94, 8.33 and 10.58 eV, can be identified as the transitions from the valance bands (3rd, 8th, 16th, 22nd and 31st, respectively) to the conduction bands (3rd, 8th, 15th, 23rd and 32nd, respectively) count from

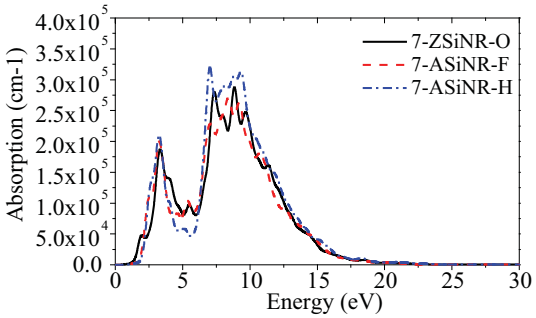

Figure 12. Absorption peaks of O-, F- and H-terminated 7-ASiCNRs.

Fermi level for 13-ASiCNRs, while for 7-ASiCNRs, the peaks are at 3.31, 4.87, 7.02, 8.76 and 10.71 eV, that is, the wider bands have somewhat red-shift. As the irradiation energy increases, the real parts of the conductance for the wider bands attenuate to zero first and maintains, that is the spectra of the conductance structures for the narrower bands are slightly richer than those of the wider bands.

The absorption of O-, F- and H-terminated 7-ASiCNRs vs. photon energy are presented in figure 12. From figure 12, we can see that the absorption peaks of all the three systems are present at two regions, which is something like the results in ref. [29] calculated using Bethe–Salpeter equation based on GW approximation. Because of the similar band structures of F- and H-terminated 7-ASiCNRs, their absorption spectra have similar shapes but different amplitudes. The absorption spectra of 7-ASiCNR-O, by contrast, has somewhat blue-shift in low energy region due to the smaller band gap. When we compare the absorption spectra of ASiCNRs with different widths, we find that the absorption spectrum is slightly dependent on the width. In detail, the wider spectrum has higher amplitude and a little red-shift.

4. Conclusion

In summary, using the first-principles PAW potential, we investigated systematically the optical properties of the 7- and 13-ASiCNRs terminated with O, F and H atoms within the DFT framework under GGA. Under the irradiation of an external electromagnetic field, we have presented that the dielectric function, reflection spectra, energy loss coefficient and the real part of the conductance are sensitive to the irradiation energy. The results show that: (1) Different terminal atoms did not make much difference in the shape of the curves of the optical constants for ASiCNR with the same width and different amplitudes; (2) the optical constants of the wider nanoribbons usually have a higher peak than the narrower ones in low energy range because the former has more electrons than the latter; (3) the optical constants are sensitive to the low-energy range, the spectra attenuate to zero except that the real part of the dielectric function maintains a constant. With the advancement of science and progress of experimental technology, O, F and H atoms terminated ASiCNRs with rich electronic and optical properties may be used to design SiC-based nanoscale photoelectric devices.

Acknowledgements

The authors would like to acknowledge the support from the Science and Technology Key Projects of Henan Province, China (Grant Nos 152102210124 and 162102310485) and Henan Province Key Scientific Research project (Grant No. 16B510004).

References

[1] N H Song, J Lv and Y Wang, *Comput. Mater. Sci.* **77**, 31 (2013)
[2] L C Ma and H S Zhao, *J. Phys. Chem. Solid* **74**, 1115 (2013)
[3] S M Pratik, A Nijarmudheen and A Datta, *J. Phys. Chem. C* **121**, 1752 (2017)
[4] C Chowdhury, S Jahiruddin and A Datta, *J. Phys. Chem. Lett.* **7**, 1288 (2016)
[5] C Chowdhury, S Karmakar and A Datta, *J. Phys. Chem. C* **121**, 7615 (2017)
[6] S Dutta, A K Manna and S K Pati, *Phys. Rev. Lett.* **102**, 096601 (2009)
[7] H Nematian, M Moradinasab, M Pourfath, M Fathipour and H Kosina, *J. Appl. Phys.* **111**, 093512 (2012)
[8] I Silveiro, Juan Manuel Plaza Ortega and F Javier García de Abajo, *Light Sci. Appl.* **4**, e241 (2015)
[9] F Afshari and M Ghaffarian, *Physica E* **89**, 86 (2017)
[10] K S novoselov, A K Geim, S V Morozov, D Jiang, M I Katsnelson, I V Grigorieva, S V Dubonos and A A Firsov, *Nature (London)* **438**, 197 (2005)
[11] H Zhang, W Q Ding, K He and M Li, *Nanoscale Res. Lett.* **5**, 1264 (2010)
[12] P Melinon, B Masenelli, F Tournus and A Perez, *Nat. Mater.* **6**, 479 (2007)
[13] X H Sun, C P Li, W K Wong, N B Wong, C S Lee, S T Lee and B K Teo, *J. Am. Chem. Soc.* **124**, 14464 (2002)
[14] H C Hsueh, G Y Guo and S G Louie, *Phys. Rev. B* **84**, 085404 (2011)
[15] H Şahin, S Cahangirov, M Topsakal, E Bekaroglu, E Akturk, R T Senger and S Ciraci, *Phys. Rev. B* **80**, 155453 (2009)
[16] E Bekaroglu, M Topsakal, S Cahangirov and S Ciraci, *Phys. Rev. B* **81**, 075433 (2010)
[17] P Lou, *Phys. Status Solidi B* **249**, 91 (2012)

[18] C Y He, X L Wu, J C Shen and P K Chu, *Nano Lett.* **12**, 1545 (2012)
[19] W Feng, J T Ma and W Y Yang, *Cryst. Eng. Commun*. **14**, 1210 (2012)
[20] R B Wu, L L Wu, G Y Yang, Y Pan, J J Chen, R Zhai and J Lin, *J. Phys. D: Appl. Phys.* **40**, 3697 (2007)
[21] I A Salama, N R Quick and A Kar, *J. Appl. Phys.* **93**, 9275 (2003)
[22] J Guan, W Chen, X J Zhao, G G Yu, X R Huang and C C Sun, *J. Mater. Chem*. **22**, 24166 (2012)
[23] P Lou, *Phys. Chem. Chem. Phys*. **13**(**38**), 17194 (2011)
[24] J M Morbec and G Rahman, *Phys. Rev. B* **87**, 115428 (2013)
[25] Y Ding and Y L Wang, *Appl. Phys. Lett.* **101**, 013102 (2012)
[26] P Lou, *J. Mater. Chem. C* **1**, 2996 (2013)
[27] Z K Tang, L L Wang, L M Tang, W Q Huang, D Y Zhang, L Xu and X F Li, *Solid State Commun*. **158**, 25 (2013)
[28] A J Du, Z H Zhu, Y Chen, G Q Lu and S C Smith, *Chem. Phys. Lett.* **469**, 183 (2009)
[29] N Alaal, V Loganathan, N Medhekar and A Shukla, *J. Phys. D: Appl. Phys.* **49**, 105306 (2016)
[30] S Y You and Y Wang, *J. Semicond.* **27**, 1927 (2006) (in Chinese)
[31] Y L Song, D B Lu, B L Cui and J M Zhang, *Pramana – J. Phys.* **78**, 469 (2012)
[32] D B Lu, Y L Song, X Y Huang, C Y Pu and Q N Pan, *Superlatt. Microst.* **91**, 31 (2016)
[33] Z F Wang, J Q Wang, Z P Li, P W Gong, X H Liu, L B Zhang, J F Ren, H G Wang and S R Yang, *Carbon* **50**, 5403 (2012)
[34] N Kumar, J D Sharma and P K Ahluwalia, *Pramana – J. Phys.* **82**, 1103 (2014)
[35] G Kresse and J Hafner, *Phys. Rev. B* **47**, 558 (1993)
[36] G Kresse and J Hafner, *Phys. Rev. B* **49**, 14251 (1994)
[37] G Kresse and J Furthmüller, *Comput. Mater. Sci*. **6**, 15 (1996)
[38] G Kresse and J Furthmüller, *Phys. Rev. B* **54**, 11169 (1996)
[39] G Kresse and D Joubert, *Phys. Rev. B* **59**, 1758 (1999)
[40] J P Perdew, K Burke and M Ernzerhof, *Phys. Rev. Lett.* **77**, 3865 (1996)
[41] D B Lu, Y L Song, Z X Yang, H R Xu, C Wang and Z H Gao, *Eur. Phys. J. B* **84**, 419 (2011)
[42] D B Lu, Y L Song, X Y Huang, C Y Pu and Q N Pan, *Superlatt. Microst.* **91**, 31 (2016)
[43] D Allali, A Bouhemadou and S Bin-Omran, *Comput. Mater. Sci.* **51**, 194 (2011)
[44] W H Liao, G H Zhou and F Xi, *J. Appl. Phys*. **104**, 126105 (2008)